

Multiscale Modeling of Cu_xAg_yAu_{1-x-y} surface segregation for propylene epoxidation

Ankit Kumar Gautam



Submitted in partial fulfillment of the requirements for the degree of
Master of Science

Department of Chemical Engineering

Carnegie Mellon University

Pittsburgh, PA, USA

December 18, 2020

Carnegie Mellon University

CARNEGIE INSTITUTE OF TECHNOLOGY

REPORT

SUBMITTED IN PARTIAL FULFILLMENT OF THE REQUIREMENTS

FOR THE DEGREE OF **Master of Science**

TITLE Multiscale Modelling of CuAgAu surface segregation for propylene epoxidation

PRESENTED BY Ankit Kumar Gautam

ACCEPTED BY THE DEPARTMENT OF

Chemical Engineering

JOHN KITCHIN, PROFESSOR AND ADVISOR

DATE



John Kitchin's signature is written in blue ink, appearing to read "John Kitchin". It is placed above his title and the date.

12/15/2020

DATE

ANNE S. ROBINSON, PROFESSOR AND DEPARTMENT HEAD

Abstract

Multicomponent alloys very often exhibit superior properties than their constituent individual metals. For an industrially relevant reaction such as propylene epoxidation, an appropriate catalyst can greatly enhance the productivity of a process. For example, Ag catalysts show excellent activity but alloying Ag with Cu or Au results in increased selectivity and conversion. For a multicomponent alloy, surface composition which largely dictates chemical activity of a catalyst, often differs from its bulk composition. This phenomena is called surface segregation and it depends on bulk concentrations, temperature and other factors. The effects of surface segregation must be carefully considered while designing a multicomponent alloy catalyst. This study is focussed on understanding the extent of surface segregation across the composition space in $\text{Cu}_x\text{Ag}_y\text{Au}_{1-x-y}$ ternary system. In this work, surface segregation is modeled via Monte Carlo simulations. To evaluate energies of intermediate configurations arising during Monte Carlo simulations, a machine learning model is trained on first principles Density-Functional Theory energies. The combination of these computational tools lets us predict the surface excess which will finally help us in tailoring the specified surface composition for the catalyst.

Keywords: Density Functional Theory, Neural Network, Monte Carlo, Multiscale Modeling, Surface Segregation, Ternary Phase Diagram

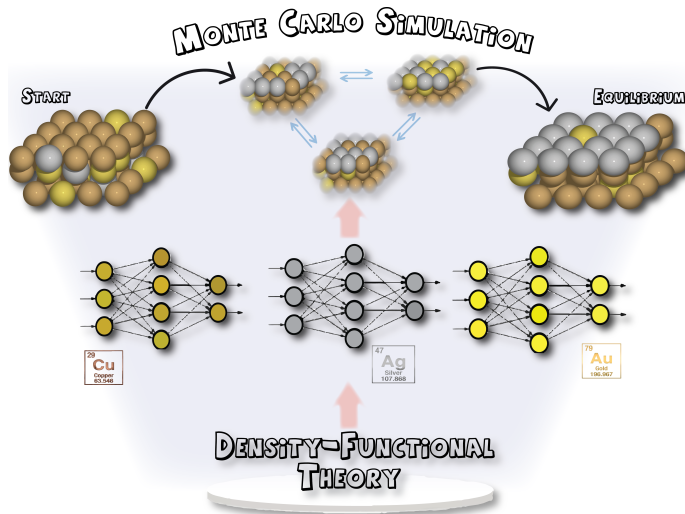


Figure 1: Graphical Abstract

Acknowledgements

I would like to thank Prof John Kitchin for his constant guidance on the project and helping me improve my scientific writing and making me a better and accountable researcher. I would like to thank my colleagues in the Kitchin-group for their contribution in making my Master's experience awesome. Specifically, I would like to thank Yilin Yang who provided me with code required and also answering a lot of my queries.

Additionally, I would also like to thank the collaborators on the DMREF project for having me on the team. The faculty members include Prof John Kitchin, Prof Zack Ulissi, Prof Andy Gellman, and Prof Jingguang Chen. The students include Zhitao Guo, Yilin Yang, Matt Adams, Will Porter.

Contents

1	Introduction	1
1.1	Surface segregation	1
1.2	Segregation in Cu, Ag, Au ternary alloys	2
1.3	Monte Carlo simulations to model surface segregation	3
2	Methods	4
2.1	Github repository	4
2.2	DFT calculations	5
2.3	Neural Network setup	6
2.4	MC canonical ensemble procedure	8
3	Results and Discussion	9
3.1	k points energy convergence	9
3.2	Ternary diagram and fingerprint space	10
3.3	Neural Network Training	11
3.4	Monte Carlo simulations	12
3.5	Discussion on surface excess values	14
3.6	Segregation energies for binary pairs from McLean equations .	14
3.7	Dispersion force contribution to AgAu segregation	16
3.8	Surface relaxation effect on Ag-Au swaps	18
3.9	Segregation on FCC 211 surface	20
3.10	Analytical solution to ternary surface segregation	21
4	Conclusions	22

List of Figures

1	Graphical Abstract	2
2	kpts convergence for energy difference for $1 \times 1 \times 7$	9
3	4000 sampled compositions across ternary space	10
4	Fingerprint space of the 4000 data points	10
5	NN performance and training data.	11
6	Interactive tool to view MC trajectories	12
7	MC trajectory for 30% Cu, 30% Ag and 40% Au	12
8	Monte Carlo Surface Excess Plot	13
9	Segregation Free Energy at Ternary Compositions	15
10	AgAu segregation energies for various vdw correction	18
11	Neural Network performance on surface relaxed structures.	19
12	Segregation on 211 surface	21
13	Analytical Surface Excess for CuAgAu ternary system	22

List of Tables

1	Input Vector for Neural Network	7
2	Comparison of various dispersion corrections to DFT	17

1 Introduction

1.1 Surface segregation

Surface segregation is the phenomenon of preferential enrichment of one species within a multi-component alloy. This leads to the surface composition of a catalyst often differing from its bulk composition. Many factors go into determining this deviation such as bulk composition, crystal facet, temperature and pressure of the system¹ or even the presence of an adsorbate on the surface.²⁻⁴ The ability to quantify surface composition provides an understanding of the underlying catalytic process. Pioneering work by McLean in 1957 for segregation in grain boundaries⁵ is still used towards modeling segregation on surfaces. For the case of a binary metal alloy, the equation goes like

$$\frac{x_1^s}{1 - x_1^s} = \frac{x_1^b}{1 - x_1^b} \exp\left(-\frac{\Delta G_{seg}^{(1)}}{RT}\right) \quad (1)$$

x_i^s in Eqn. 1 denotes surface composition (mole fraction) of component i and x_i^b represents its bulk composition. $\Delta G_{seg}^{(i)}$ in these equations represents the free energy change related to segregation of component i to the surface for one mole of atoms. T is the temperature in Kelvin. The equations can be extended to a ternary case as follows:

$$\frac{x_1^s}{1 - x_1^s - x_2^s} = \frac{x_1^b}{1 - x_1^b - x_2^b} \exp\left(-\frac{\Delta G_{seg}^{(1)}}{RT}\right) \quad (2)$$

$$\frac{x_2^s}{1 - x_1^s - x_2^s} = \frac{x_2^b}{1 - x_1^b - x_2^b} \exp\left(-\frac{\Delta G_{seg}^{(2)}}{RT}\right) \quad (3)$$

In these equations, $\Delta G_{seg}^{(i)}$ is the big unknown that goes into the equations currently as the two non-linear equations can be readily solved together. Efforts to model ternary segregation energy started with Hoffmann and co-workers⁶ using regular solution nearest neighbor bond model.⁷ Their work on dilute ternary systems viewed ternary systems as deviations from a binary

system.^{8,9} They also shed light on phenomena such as “cosegregation” and “site competition” useful for ternary segregation. Cosegregation occurs when the attractive forces from two surface-active (components which tend to segregate) enrich the surface together. Whereas site competition is observed when both surface-active solutes have large enough concentrations capable of flooding the surface but there is a maximum amount of total surface entities. Moreover, ternary segregation can not be interpreted as binary segregation between the two surface-active components, as Good et al.¹⁰ also remarked from their results of the CuAuNi ternary system. Good’s work showed that in binary cases, Au and Cu segregated in Au-Ni and Cu-Ni system respectively and Au segregates in Au-Cu system. But, this knowledge cannot be extrapolated to conclude that Au would be the dominant surface component. Ternary interaction is much more complex than what one expects to be.¹¹

Surface segregation is often modeled as surface-active species being solutes in a solvent. Because of such *impurities* various strain effects evolve to drive surface-active species towards the surface to obtain thermodynamically more stable structure. To obtain segregation energies, a model named ‘Atom Exchange Method’ has been used in different forms over the years starting from Mclean,⁵ Defay et. al.,¹² Wynblatt and Ku¹¹ and others. A most recent development by Zhao and co-workers^{13,14} is explained and replicated later in this work.

1.2 Segregation in Cu, Ag, Au ternary alloys

We focus our study on the design of catalyst intended for propylene epoxidation. Propylene oxide (PO) is a heavily used intermediate in the chemical industry. PO is produced from the oxidation of propylene. At present, the two dominant methods of production are the chlorohydrin process and the hydroperoxide process. Both of the processes suffer from disadvantages such as the use of expensive Cl₂ in the former and safety issues in the latter. A

relatively new process of direct epoxidation is of more interest to researchers because of improved productivity.

Silver rich catalysts have long been in use for the oxidation of alcohol¹⁵ but they suffer from selectivity for epoxidation.^{16,17} This occurs because the route of production moves towards undesirable Carbon-dioxide (total oxidation).¹⁸ High selectivities have been observed by Ag addition on supported Cu catalysts,^{19,20} Au addition onto TS-1 support,^{21,22} and AuAg bimetallic catalyst.²³ This naturally raises the possibility of presence of a ternary system with both improved selectivity and conversion. This approach would require one to enumerate all possible combinations and then choose the best candidate among them.

1.3 Monte Carlo simulations to model surface segregation

To the best of our knowledge, no work till now has explicitly calculated/measured CuAgAu segregation across the whole ternary space. Experimental work by Hoffmann et al.⁸ represent only dilute values with Ag and Au composition of less than 6%. Bozzolo–Ferrante–Smith (BFS) method²⁴ has been used to study CuAgAu through a mean field approach by fitting experimental properties of the binary systems is also used for dilute compositions.

First-principles Density-Functional Theory (DFT) provides increased accuracy when compared to other techniques such as Embedded Atom Method (EAM), ReaxFF etc. although at a cost of computational expense. Fortunately, this hindrance has been growing smaller with more advancements in computational techniques including that of machine learning and artificial intelligence. It has been shown that machine learning can be applied to capture the underlying high dimensional potential energy surface.^{25,26} This allows us to use results comparable to DFT without conducting a DFT calculation. This idea of using a surrogate model of DFT brings down the computational cost up to 5 orders of magnitude.^{26,27} Such a drastic reduction is partially

achieved by implementing a cutoff radius to neglect faraway interactions. Specifically, we utilized the Behler-Parinello Neural Network (BPNN) framework trained on DFT data. This procedure has been validated for Au,^{28,29} Cu,^{30–32} and Ag.^{33,34} This review by Prof. Behler³⁵ provides a comprehensive list of other materials also modeled using BPNN. Finally, this NN is used to quickly predict energies encountered within MC simulation, ultimately used to obtain surface compositions.

This work studied surface segregation by carrying out Monte Carlo (MC) simulations in a canonical ensemble utilizing a machine-learned potential trained on DFT calculations. 4000+ DFT calculations were performed to cover the entire composition and configuration space. A Neural Network with 2 hidden layers and 10 nodes in each layer is trained on the DFT data. The Neural Network easily achieves the desired accuracy and demonstrated a similar Mean Absolute Error (MAE) on validation and test data. MC simulations were carried out for 20000 successful swaps to equilibrate the bulk and surface interaction. Surface excess plots were generated to survey surface segregation at various points of ternary space. Using the surface and bulk compositions, segregation energy at all compositions were evaluated using the Langmuir-Mclean equations as given in Eqn. 2.

2 Methods

2.1 Github repository

The code required to fully reproduce the results of this work is made available at <https://github.com/gautamankitkumar/ankitgau-ms-report-data>. The repository contains python code in Jupyter notebooks with detailed comments. The links at the top of each notebook contains a hyperlink to Google Colab which executes python code on the cloud thus requiring no installation on the reader’s computer. The notebooks were saved in an executed state so

that the reader can just read through the notebooks or play around with the code as they please.

2.2 DFT calculations

Density Functional Theory calculations were performed using the Vienna *ab initio* simulation package (VASP)^{36–38} with the Perdew\$Burke\$Ernzerhof Generalized Gradient Approximation (GGA-PBE)^{39,40} exchange-correlation functional. Core electrons were described using the projector augmented wave (PAW) potentials.^{41,42} MonkhorstPack k -point grids⁴³ were chosen to have minimum 450 per reciprocal atom and planewave cutoff of 400 eV was selected. These settings give out a convergence error of below 2 meV/atom when comparing difference in energies. Different sized slabs were created at varying lattice constants as follows:

- 100 of $1 \times 1 \times 7$,
- 100 of $2 \times 1 \times 7$,
- 200 of $\sqrt{3} \times \sqrt{3} \times 7$,
- 200 of $\sqrt{7} \times \sqrt{7} \times 5$,
- 200 of $3 \times 3 \times 5$

The 5 lattice constants varied between the smallest (Cu, 3.63 Å) and the largest (Au, 4.17 Å) and were equally spaced so that the Neural Network learns to capture the underlying potential energy surface at different lattice constants. Thus, in total 4000 training data points were generated.

Various types of van der Waals corrections to Perdew-Burke-Ernzerhof exchange-correlation functional (PBE) were tested for Ag-Au binary segregation. These include DFT-D2 proposed by Grimme et al.,⁴⁴ DFT-D3,⁴⁵ and Bayesian Error Estimation Functional with van der Waals (BEEF-vdW).⁴⁶

The above-mentioned corrections were easily implemented in Vasp by setting the `ivdw` parameter to corresponding values.

2.3 Neural Network setup

Since DFT calculations are computationally expensive, a surrogate machine learning model was built to predict the energy of an unknown configuration. To this end, a Behler Parinello Neural Network framework (BPNN)²⁶ was used to obtain energies of the surface slabs, where slabs are first transformed to fingerprint space through G^2 symmetry functions.⁴⁷ These symmetry functions work very well to capture the atomic environment around an atom. Information of the chemical identities and positions of each atom is encoded within the symmetry functions. Such a transformation is necessary to make the energy model invariant to translation, rotation, and the permutation of atoms. G^2 values use a cutoff function to remove the interaction of faraway atoms. A cutoff function $f_c(R_{ij})$ where R_{ij} is the distance between atom i and atom j is defined as follows:

$$f_c(R_{ij}) = \begin{cases} 0.5 \times \left[\cos\left(\frac{\pi R_{ij}}{R_c}\right) + 1 \right] & \text{for } R_{ij} \leq R_c \\ 0 & \text{for } R_{ij} > R_c \end{cases} \quad (4)$$

A `cosine` function is applied to exploit the smooth decay to value of zero at $r = R_c$. A single NN is trained for each distinct chemical species, in this case, each one for Cu, Ag, and Au. G^1 and G^2 for an element with the atomic number Z centered at atom i is written as follows:

$$G_i^{1,Z} = \sum_j^Z f_c(R_{ij}) \quad (5)$$

$$G_i^{2,Z} = \sum_j^Z e^{-\eta(R_{ij}-R_s)^2} f_c(R_{ij}) \quad (6)$$

where the sum for j goes over for all atoms with atomic number Z which only accounts for atoms present inside a cutoff sphere. η, R_s were user-defined hyperparameters which were fixed for values of $\eta = 0.05, 4, 20, 80$ and $R_s = 0$ for each η in this work. The role of η and R_s was to give different values for same input of R_{ij} . This vector of 4 values of symmetry functions is unique for each structure and avoids the problem of the same energy for different configurations.⁴⁷ The cutoff radius was set as $R_c = 6\text{\AA}$ for each symmetry function as they work well for the chosen metal species.^{29,30}

For our case of three species, the final input vector to Neural Network had a 12×1 shape containing the following quantities as enumerated in Tab. 1. There exist many other descriptors to represent an atomic environment

Table 1: Input Vector for Neural Network

Cu	G^2 for $\eta = 0.05, R_s = 0$ G^2 for $\eta = 4, R_s = 0$ G^2 for $\eta = 20, R_s = 0$ G^2 for $\eta = 80, R_s = 0$
Ag	same as Cu
Au	same as Cu

including the Coulomb Matrix,⁴⁸ Ewald sum Matrix,⁴⁹ Sine Matrix,⁴⁹ Many Body Tensor Representation,⁵⁰ Smooth Overlap of Atomic Orbitals.⁵¹ A very nice compilation of these descriptors are available in Himanen's work⁵² and maintained online as a plug and play model as a python package.

All the NNs had the same architecture of 2 hidden layers with 10 hidden nodes each. The training was done over 80% of the data and 20% was left as validation and test data. The learning rate was set to be equal to 0.1 and the convergence criteria were set to achieve Mean Absolute Error of 2 meV/atom for the NN. No force training was carried out as we were only interested in energy prediction. The training was conducted in a code written in Pytorch⁵³ and atomic simulation environment(ase).^{54,55}

2.4 MC canonical ensemble procedure

Metropolis Monte Carlo simulations were performed with starting compositions spread throughout the ternary space. 20000 successful atomic swaps are carried out in a single simulation. A slab size of $10 \times 10 \times 15$ was used at a temperature of 600 K. An atom and one of its (different specie) neighbors were chosen randomly at each time step for a potential swap. Energy for the two structures, the original and one evolving because of the swap, was predicted using the trained NN. A successful swap was considered when the total energy was lowered due to the swap. A swap was also accepted by Boltzmann probability criteria. The full algorithm is described in Algorithm 1.

Algorithm 1: Monte Carlo algorithm

Result: Equilibrium Surface composition

Input

T : Temperature in Kelvin

X_{Cu}, X_{Ag}, X_{Au} : Starting compositions for each element

Initialize Successful_Steps = 0;

while Successful_Steps \leq 20000 **do**

$Atom1 \leftarrow SelectAtomAtRandom()$

$Atom2 \leftarrow SelectAtom1'sNeighbor()$ //Different Specie

$Temp_Configuration \leftarrow Switch Atom1 and Atom2$

$E_1 \leftarrow Energy(Original_Configuration)$

$E_2 \leftarrow Energy(Temp_Configuration)$

$\Delta E \leftarrow E_2 - E_1$

$h \leftarrow Random(0, 1)$ //UniformRandomNumber

if $\Delta E \leq 0$ or $h \leq exp\left(-\frac{\Delta E}{k_B T}\right)$ **then**

 Update Successful_Steps+=1;

$Original_Configuration \leftarrow Temp_Configuration$

end

This algorithm described the state of the entire slab at each iteration and its composition (including layer-by-layer) information was recorded at 100 step intervals. Using the average of last 40 values, the final state of the slab was obtained and surface excess (final-initial composition) plotted at each data point.

3 Results and Discussion

3.1 k points energy convergence

Appropriate k points were chosen to get a converged energy difference. Two slabs of size $1 \times 1 \times 7$ were created and energy between the two were compared for different pairs of metals. Fig. 2 shows how the energy difference changed with different k points setting. Based on the computational time vs accuracy compromise, $k = 10$ was chosen in x and y for bulk calculations.

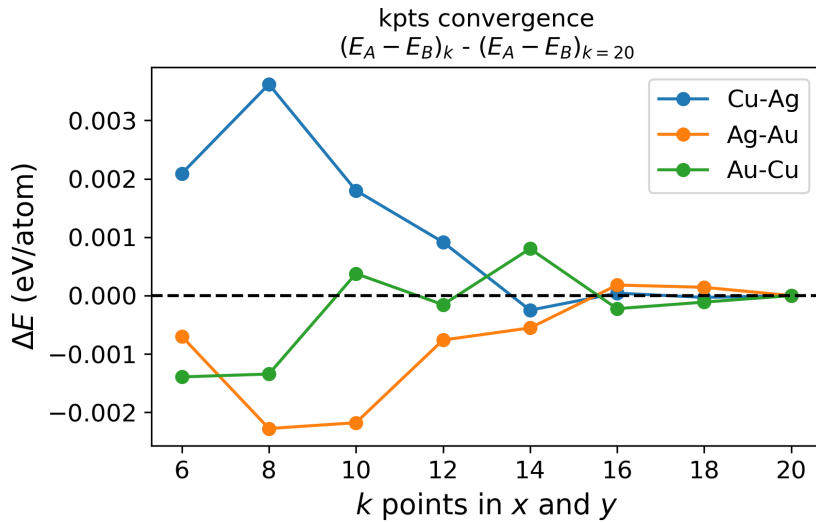


Figure 2: kpts convergence for energy difference for $1 \times 1 \times 7$

3.2 Ternary diagram and fingerprint space

DFT calculations on slabs with sizes as mentioned in Sec. 2.2 were carried out with randomized compositions. Dirichlet sampling was used to generate the sampling points. The sampled compositions were plotted as shown in Fig 3. And since these points would go into the Neural Network input space, the

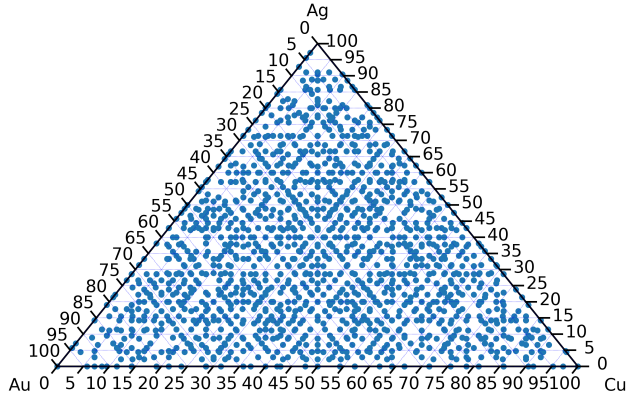


Figure 3: 4000 sampled compositions across ternary space

fingerprint space was also plotted as shown in Fig 4.

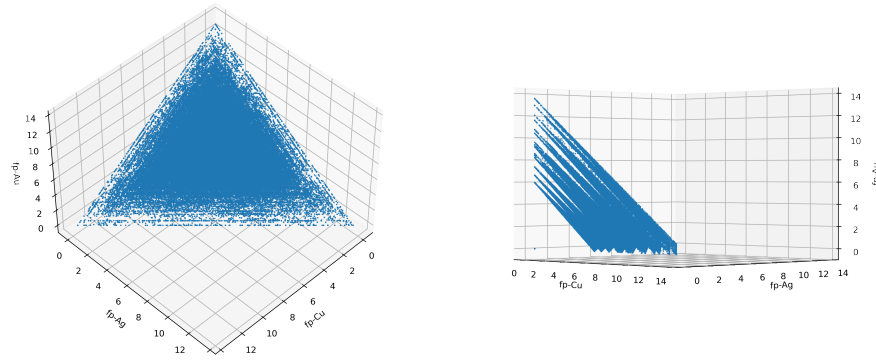


Figure 4: Fingerprint space of the 4000 data points

These two plots show that the chosen composition points covered the ternary space entirely.

3.3 Neural Network Training

NN training was conducted on 80% of the data with a convergence criterion of Mean Absolute Error (MAE) of 2 meV/atom. Validation and test data were separated from training data to provide the measure of performance of NN on unseen data. The Neural Network performs very well and achieved almost similar MAE on unseen data. The NN accuracy was not affected much when any of the parameters such as NN architecture, learning rate or number of epochs is changed. NN training on the data is summarized in Fig. 5.

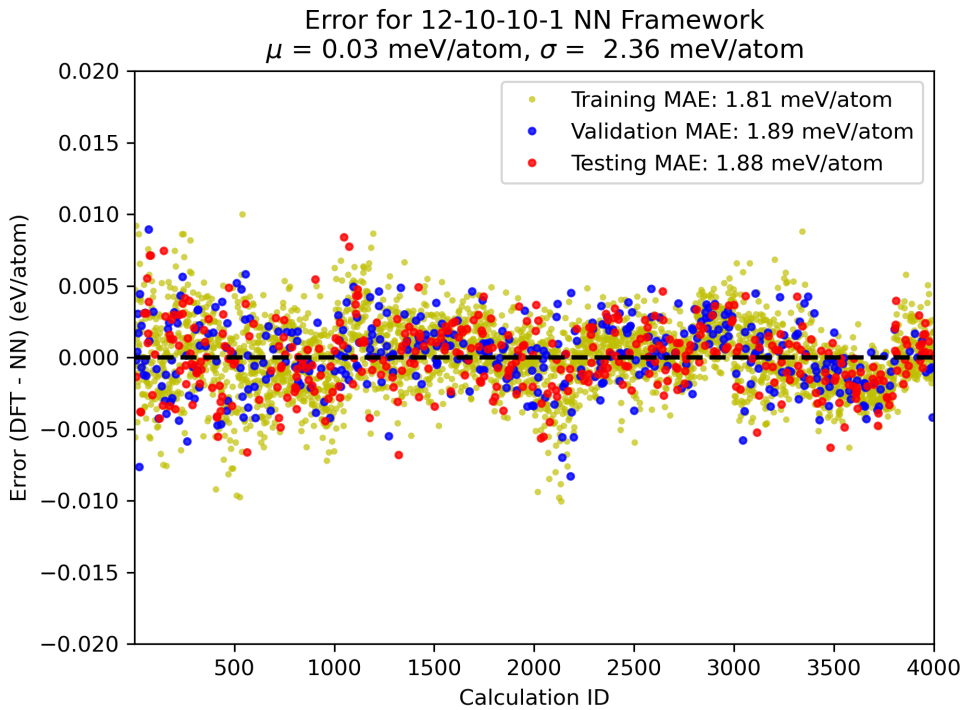


Figure 5: NN performance and training data.

The trend in the MAE occurs partly because the training data itself is structured. The standard deviation of 2.5 meV/atom shows that the spread around zero is very small. For comparison, segregation energies for Cu in Au and Ag are found to be 0.22 eV and 0.34 eV respectively. The other segregation energies are also of similar magnitude.⁵⁶

3.4 Monte Carlo simulations

Monte Carlo simulations were carried out at composition intervals of 10%, i.e. (0,10,90), (0,20,80) and so on. Simulations were carried out for 20000 steps which are chosen as the time when all the favorable swaps have already occurred and equilibrium is achieved. This sampling on compositions was dense enough to capture the underlying surface excess trend. To aid the visualization process, an interactive graph in Plotly⁵⁷ was created in Jupyter notebooks. When a user clicks on a point in Fig. 6a, a plot is generated as seen in Fig. 6b, which is the desired Monte Carlo trajectory.

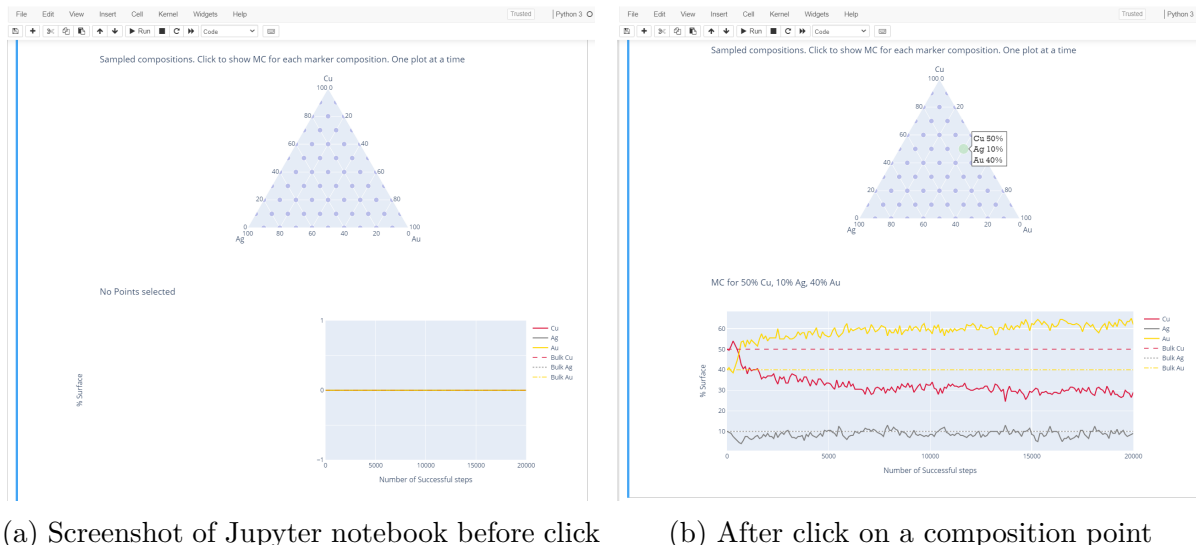


Figure 6: Interactive tool to view MC trajectories

A single sample image from for a clicked image is shown in Fig. 7. Notice how in this given case, gold surface composition shoots up and copper surface composition goes down. This composition shows a case of gold segregation to the surface and copper dissolution into the bulk. The surface excess was calculated as difference between the fi-

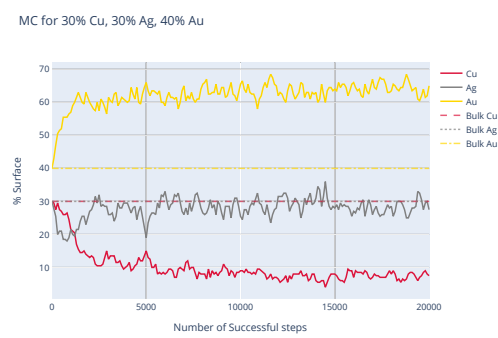


Figure 7: MC trajectory for 30% Cu, 30% Ag and 40% Au

nal composition and initial composition for each point. The initial composition of the surface was equal to the bulk composition of the composition of interest. The final composition was taken as the average of last 40 values i.e. time steps 16000 to 20000. This gave a discrete set of values of each element on each sampled point within the ternary diagram. The contour plots were generated used `matplotlib`'s `tricontour` and `tricontourf` functions. The obtained surface excess plots are shown in Fig. 8.

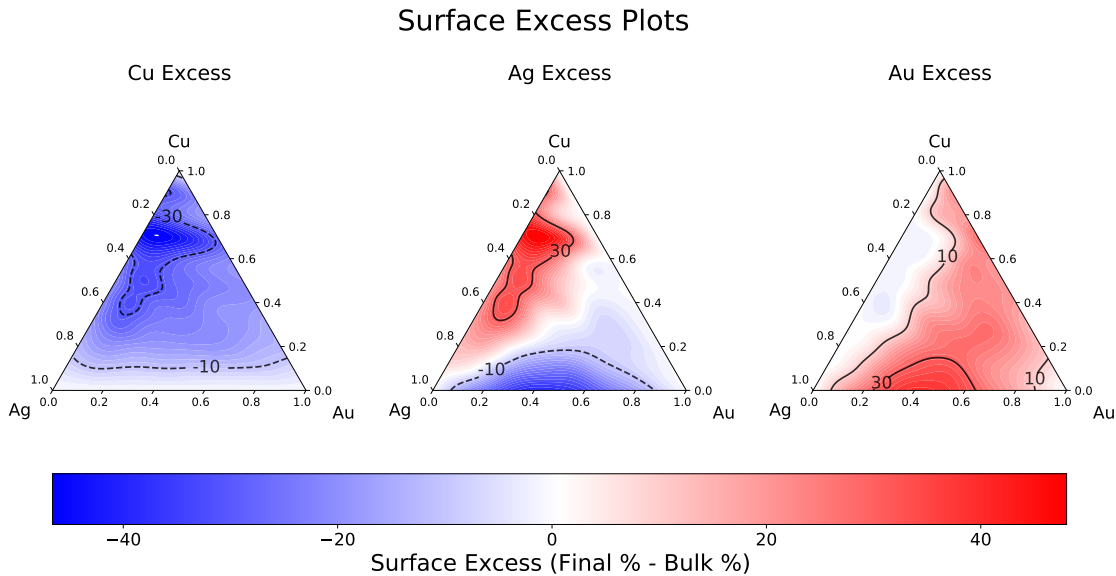


Figure 8: Monte Carlo Surface Excess Plot

One reads the above plot by selecting a point on the ternary phase diagram, which fixes the initial surface composition and then matching the color observed at that point with the color scale drawn at the bottom. Wikipedia has an excellent guide to read values from a ternary plot. Now, the three plots give excess values for the three species i.e Cu, Ag, and Au. For the case of copper excess (leftmost), picking almost any point is blue-colored which means that our model predicted copper to move into bulk and reduce its composition from its initial composition.

3.5 Discussion on surface excess values

To justify the results obtained, understanding segregation phenomena is important. Segregation energy (and thus the segregation behavior) stems from mainly these three main contributions as per atom-exchange method.⁶ These are differences in surface energies, Mixing behavior of the participating metals and, Solute elastic strain. Treglia et. al.⁵⁸ remarked that segregation in 95% of bimetallic systems could be explained solely by the first contribution of difference in surface energies. The rest 5% is constituted by cases where a huge size difference exists between the elements. Copper mixing into the bulk was correctly predicted when present in a mixture either of gold or silver. The copper dissolution into the bulk was also observed over the years, both experimentally,^{8,14,59,60} and computationally.^{56,61,62} Silver segregation in copper-rich regions was correctly predicted (similar argument as above) but silver dissolution in gold-rich areas was contradictory to what is observed experimentally. This discrepancy is further explored in a subsequent section in more detail. Gold segregation in copper-rich regions is rightly predicted (but exaggerated) as also observed experimentally^{8,63–65} and computationally^{9,56}

3.6 Segregation energies for binary pairs from McLean equations

Assuming the segregation behavior as three binary surface segregation events occurring together, the following three equations can be written:

$$\text{Cu}_{\text{bulk}} + \text{Ag}_{\text{surf}} \rightleftharpoons \text{Cu}_{\text{surf}} + \text{Ag}_{\text{bulk}} \quad K_{\text{CuAg}} = \frac{y_{\text{Cu}}x_{\text{Ag}}}{y_{\text{Ag}}x_{\text{Cu}}} \quad (7)$$

$$\text{Ag}_{\text{bulk}} + \text{Au}_{\text{surf}} \rightleftharpoons \text{Ag}_{\text{surf}} + \text{Au}_{\text{bulk}} \quad K_{\text{AgAu}} = \frac{y_{\text{Ag}}x_{\text{Au}}}{y_{\text{Au}}x_{\text{Ag}}} \quad (8)$$

$$\text{Au}_{\text{bulk}} + \text{Cu}_{\text{surf}} \rightleftharpoons \text{Au}_{\text{surf}} + \text{Cu}_{\text{bulk}} \quad K_{\text{AuCu}} = \frac{y_{\text{Au}}x_{\text{Cu}}}{y_{\text{Cu}}x_{\text{Au}}} \quad (9)$$

where x denotes bulk (initial) composition and y represents final surface composition (fraction). The ordering of elements is kept such that when combined, the equilibrium constants can be multiplied to unity.

$$K_{\text{CuAg}} K_{\text{AgAu}} K_{\text{AuCu}} = 1$$

x and y in Eqn. 7 were readily obtained from the Monte Carlo data and thus, utilized to calculate equilibrium constants for each case. Within each case, only data points where the composition of each component is no less than 20% was taken to avoid numerical instabilities in calculating equilibrium constants. For a case of an example pair of metals A (initially in bulk) and B (initially on surface), the segregation free energy was then calculated using $\Delta G_{seg,AB} = -RT \ln(K_{AB})$. Using R as $8.314 \frac{J}{molK}$ and $T = 600K$, we estimated segregation energies across the ternary space. The plot is available at Fig. 9.

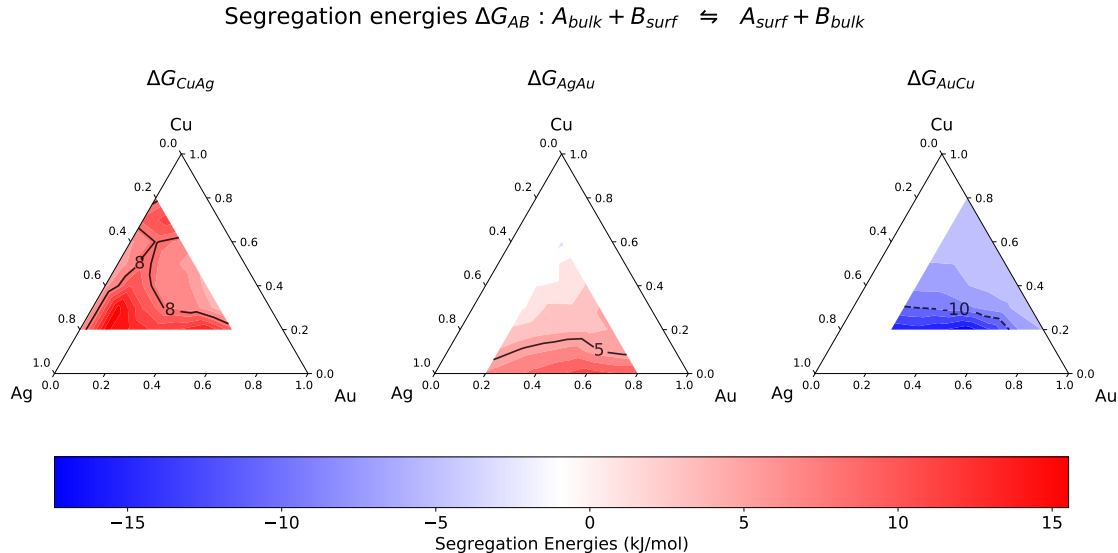


Figure 9: Segregation Free Energy at Ternary Compositions

The segregation energy values calculated here were roughly in the same order of magnitude as those reported earlier in the literature. CuAg segregation energy is reported as 0.22 eV/atom⁵⁶ which is roughly 21.2 kJ/mol.

Fig 9 shows values ranging from 0 to 15 kJ/mol which is fairly close and would deviate because of ternary interaction. We observed AgAu segregation energies in the range 0 to 7 kJ/mol while it is reported as 0.00 eV/atom and classified as mild or no segregation. Not only is the value incorrect but the segregation trend is not what is observed experimentally. AuCu segregation was seen as always negative and varied from -5 to -15 kJ/mol and it is described as -0.29 eV/atom⁵⁶ which becomes -28 kJ/mol. The segregation trend of CuAg and AuCu was obtained correctly while for the AgAu case it appeared in contrast to previously known values. More discussion on AgAu segregation takes place in a subsequent section.

3.7 Dispersion force contribution to AgAu segregation

As seen in the previous two sections, for the AgAu binary pair, Au was predicted to segregate to the surface. Based on surface energies values one would predict Ag ($\gamma = 1.172 J/m^2$)⁶⁶ to segregate with Au ($\gamma = 1.283 J/m^2$)⁶⁶ segregation because of its lower surface energies. Various experimental studies report zero^{67,68} and moderate Ag segregation.^{69? -73} But, on the other hand, computational methods predict Ag segregation^{74,75} and also Au segregation.⁷⁶⁻⁷⁹

It has been suggested that for these two metals that the surface properties are dependent on correctly including van der Waals (vdw) forces by a study by Rehr et. al.⁸⁰ The authors explain how polarization forces contribute upto 14% and 17% to cohesive energies of Ag and Au respectively. Dispersion forces are present everywhere which must be surely included in small energy differences calculations. Although weak in nature, they are important features of some selective problems. Various dispersion corrections to DFT energies have been suggested over the years with most of them gaining popularity in the last couple of decades.⁸¹ Klimes et. al. provide a great summary of different versions (complexity) of vdw corrections that have been

employed to better predict properties such as adsorption energy or binding energy among many others. In the simplest form, vdw corrections take the form of the following equations:

$$E_{\text{tot}} = E_{\text{DFT}} + E_{\text{Disp}}$$

$$\text{where, } E_{\text{disp}} = - \sum_{A,B} \frac{C_6^{AB}}{r_{AB}^6}$$

The corrections seek to capture the $\frac{1}{r^6}$ attraction term present within interaction of particles. The coefficient C_6 depends on the pairs of elements A, B in consideration. Table 2 (adapted from Klimes work⁸¹) highlights some of the vdw corrections that were incorporated in current work in pursuit of better explanation of the contradictory AgAu segregation. DCACP stands for Dis-

Table 2: Comparison of various dispersion corrections to DFT

vdw Correction	Complexity	C_6 depends on	Additional computational cost
DCACP	0	N/A	None
DFT-D2 ⁴⁴	1	Constant	Small
DFT-D3 ⁴⁵	2	Structure	Small
vdW-DF2 (BEEF) ⁴⁶	3	Density (calculated)	50%

ersion corrected atom centered potentials. BEEF stands for Bayesian error estimation functional. Each of these has its advantages for modeling different situations. Briefly, the DFT-D2 proposed by Grimme et al.⁴⁴ method is the simplest correction to DFT energies. It suffers from shortcomings such as constant corrections, diverging contribution to correction, and the correction only capturing $1/r^6$ dependence.⁸¹ DFT-D3 is the modern version developed by Grimme et al.⁴⁵ which is environment-dependent and interpolates value of C_6 based on the neighbors experienced by the atom at hand. DFT-D3 is appropriate for surfaces and adsorbed species and bulk properties.⁸² More neighbors are thought to have a squeezing effect on the central atom and it becomes less polarizable leading to a decrease in C_6 . BEEF gives out nonlocal correlation energy and the ensemble of functionals naturally gives out errors in en-

ergy

Each of these functionals was utilized to find the Ag segregation and Au segregation trend to investigate if including vdw force changes segregation behavior. Values obtained were plotted in Fig. 10. It was seen from the observed values that three of the four methods employed here predicted favorable Au segregation. Only the D2 method of vdw correction predicted experimentally correct Ag segregation. It should be noted that DFT-D2 does give better predictions for some lattice parameters and bulk properties but it often overestimates vdW interaction in almost every system.⁸³ With that fact in mind, it can be concluded that first-principles DFT calculations even after including vdw corrections suggest Au segregation. This statement is in complete contrast to what is observed experimentally. Although this is not the first reporting of this surprising behavior. Work by Hoppe et. al.⁸⁴ compared AgAu segregation to great extent by employing various vdw corrections within DFT. The authors also report the Au segregation observed in their case. This mismatch observed with experiments calls for more efforts to this development and carrying out the study using more complex DFT methods.

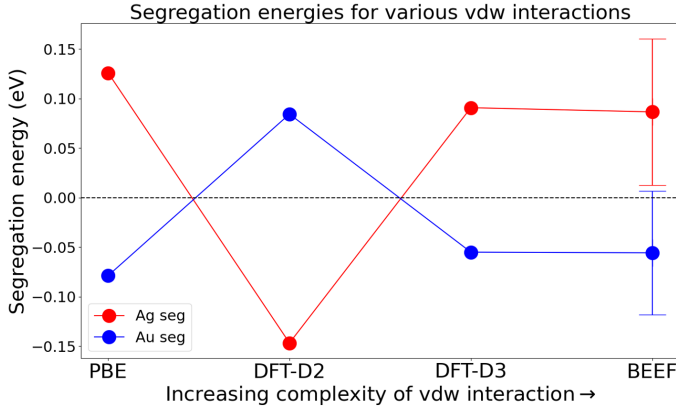


Figure 10: AgAu segregation energies for various vdw correction

3.8 Surface relaxation effect on Ag-Au swaps

To further investigate the mismatch of AgAu segregation, the trained Neural Network model was tested on structures with surface layers relaxed. The study employed here compares the energy predictions of atomic swaps that

occur within DFT surface relaxed versus the Neural Network trained on unrelaxed structures. A $2 \times 2 \times 5$ slab is taken and its bottom 3 layers are fixed and set to a composition of 1:1:1 (all atoms being present). Within the top two layers, 8 sites were to be occupied with either Ag or Au. This arrangement can be done in 256 ways. These arrangements were enumerated to have 256 energy unique structures. DFT energies were obtained for the first 50/256 structures, and ‘swap neighbors’ identified among them. Here the term swap-neighbor refers to two structures among the 256 possible, where the second structure can be obtained from the first one by a swap of only one atom. Among the 1792 possible swap-neighbors, only 176 swaps were possible within the first 50 structures. The energy predictions from the two cases are shown in Fig. 11.

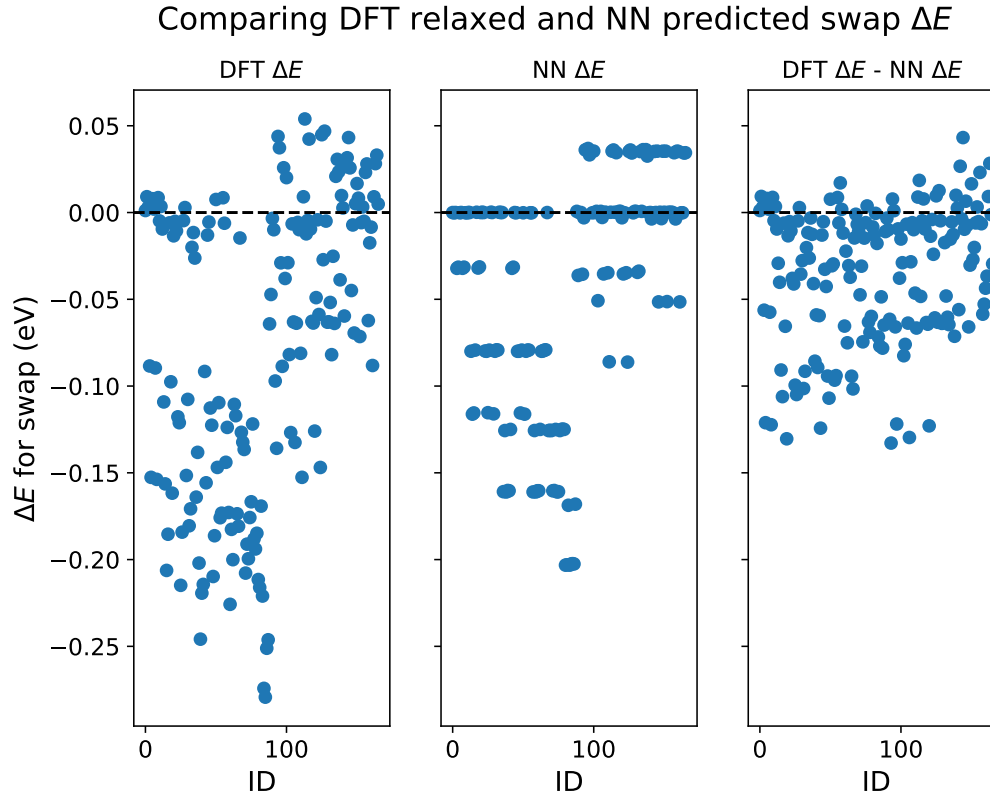


Figure 11: Neural Network performance on surface relaxed structures.

It was observed that energies of the swaps were between -0.30 eV and

0.05 eV. Neural Network predicted energies were also within the same range. More importantly, their differences varied over a smaller range from -0.13 eV to 0.05 eV. This reduction in the range of energy variation hints towards the fact that Neural Network was able to understand the underlying trend regarding relaxed structures. Since we were interested in segregation phenomena, it is the sign of ΔE_{swap} that favors or rejects an atomic swap. We compared the sign of our Neural Network predictions to that of relaxed DFT calculations by looking at the product of `sign(NN)` and `sign(DFT)`, where `sign()` is the signum function. For an atomic swap in consideration, the two should share the same sign if the product is +1. We divided the 172 possible combinations into cases that represent inter-layer exchange and intra-layer exchange. The atomic swap occurring in inter-layer exchange contributes to segregation results, while intra-layer exchanges do not. From this analysis (refer to notebooks online for plots) it was seen that most of the inter-layer exchanges share the same sign. This points to the fact that our Neural Network although trained on unrelaxed structures, accurately captures the same sign behavior as that of relaxed DFT energy predictions. Thus, in an attempt to investigate the source of AgAu segregation mismatch, the effect of surface relaxation can be safely ignored.

3.9 Segregation on FCC 211 surface

The other common source of segregation change is that experimentally, it is not always that we'll get FCC111 surfaces. As reported in Priydarshini et al.,⁸⁵ FCC111 was preferred for Cu, but other facets like 100, 110 also existed. In all of our computations, we had assumed FCC111 everywhere. To explore the segregation trend, we carried out a simulation with a $3 \times 3 \times 5$ slab and studied segregation energy for each binary pair possible in CuAgAu ternary system. The results are shown in Fig. 12

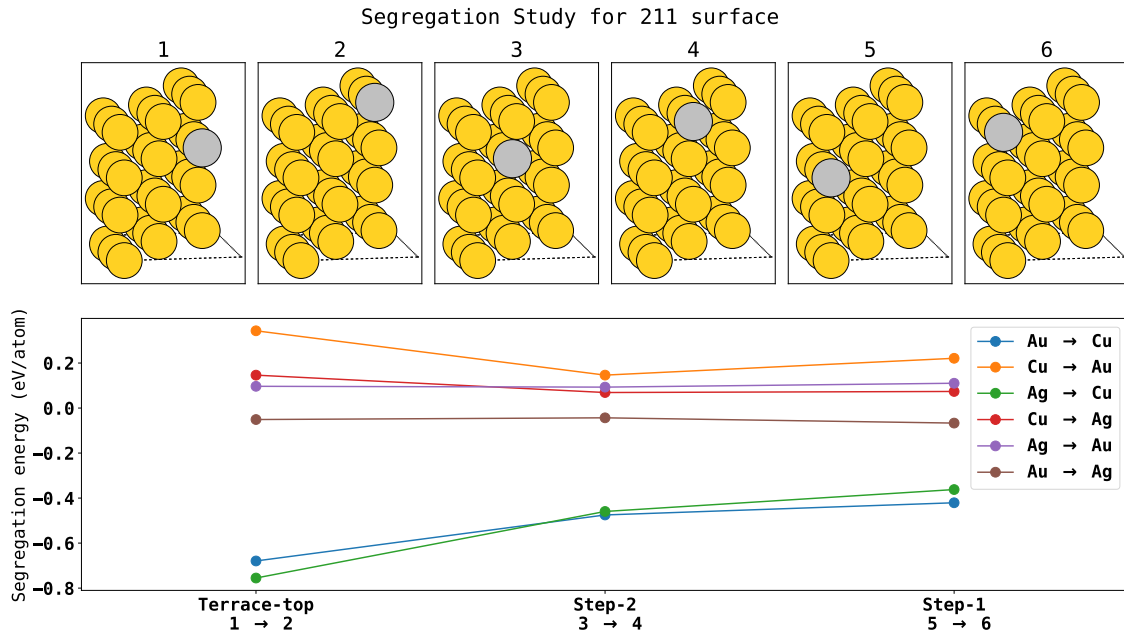


Figure 12: Segregation on 211 surface

The figure shows that there is no surprising change of segregation trend in any pair. For the case of Ag-Cu and Au-Cu the segregation got even stronger and the Ag-Au case still represents very mild segregation of Au. This study concluded that even after considering the possible inclusion of FCC211 surface, the incorrect segregation trend of AgAu cannot be explained properly.

3.10 Analytical solution to ternary surface segregation

To model the segregation analytically, Langmuir-Mclean equations were used. Zhao and co-workers¹⁴ have extended the Langmuir-Mclean equations to model ternary surface segregation energies at all compositions. This model was originally developed for CuAgPd but can be extended for the CuAgAu case. The reader is referred to the paper for full details of the equations. The authors provided a set of parameters for the elements: Pd, Ag, Au, Cu, Ni, Pt, and H in their previous work.¹³ Briefly, segregation energy for changing compositions are calculated using formulas outlined in their previous work.

Calculations were setup using these equations to obtain Fig 13 similar to Fig 8.

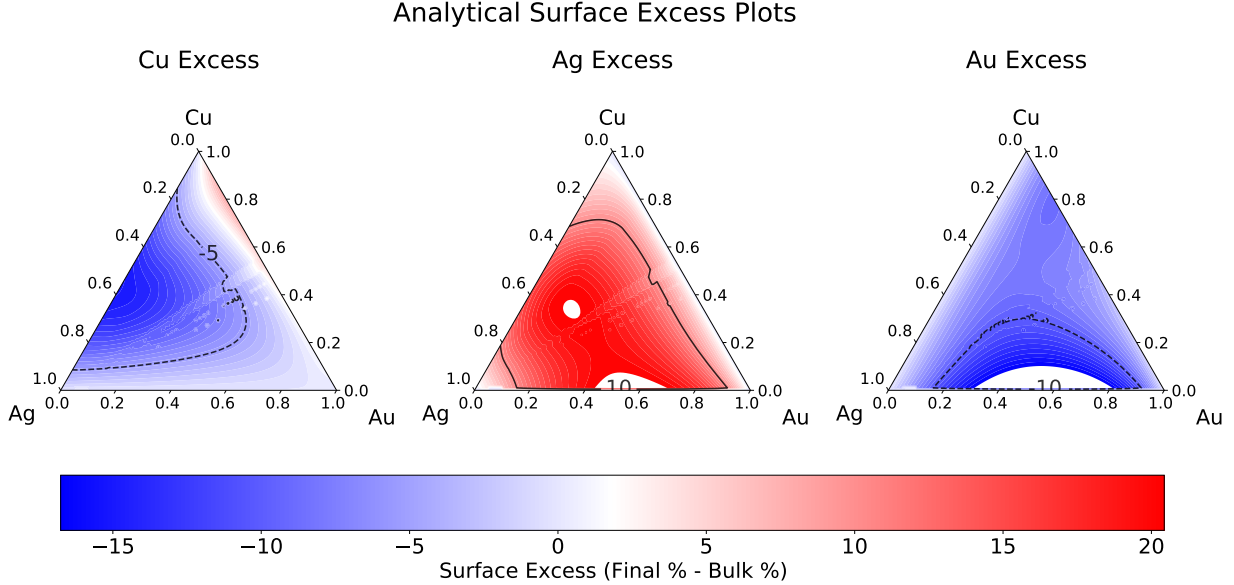


Figure 13: Analytical Surface Excess for CuAgAu ternary system

This analytical model did not predict the right segregation behavior but it captured the experimental trend of Ag being surface-active and Au being the second surface-active component. In their implementation for CuAgPd, the authors introduced an approximation in this exact model to better fit the experimental results. The approximation is included to tune the interaction between two metals. Modifications such as these can be used to fit the experimental results to prepare a more robust computational model. Authors themselves get poor extensibility to CuAgAu and it is evident from our implementation too. More work needs to go into the development of this model to predict segregation energy to attain better results.

4 Conclusions

To study surface segregation on a ternary system of CuAgAu, we utilized a Neural Network (NN) trained on Density Functional Theory (DFT) energies

within Monte Carlo (MC) simulations. 4000 energy unique DFT calculations were used as input to the NN to capture the underlying potential energy surface. The NN demonstrated very high accuracy on unseen data, possessing MAE as low as 2 meV/atom. Monte Carlo simulations at a diverse set of compositions were executed to obtain equilibrium surface composition at each of those data points. For each of these points, the surface excess for each component (Cu, Ag, and Au) was calculated and displayed as three ternary figures. Ag segregation was seen as the strongest with Au being the second surface active specie. Copper displayed a tendency to move towards the bulk at all compositions if present on the surface initially. The obtained segregation trends are in parity with the results reported in the literature except Au segregation predicted in the presence of Ag.

The segregation discrepancy of Ag and Au was further investigated by including van der Waals (vdw) force correction in DFT. It was seen that complexity of vdw force correction changes the AgAu segregation but the more complex corrections concluded with favorable Au segregation. This result was in contrast to what has been observed experimentally over the years. However, computationally, Au has been predicted to segregate in presence of Ag. To further explore the reasons for this mismatch of results, NN performance on surface relaxed AgAu atomic swaps were analyzed. It was concluded that the NN although trained on unrelaxed structures, predicted correct energy change corresponding to atomic swaps in between layers. Furthermore, segregation trends on the FCC211 surface were also calculated in an attempt to reason AgAu segregation mismatch.

Binary segregation energies were calculated by writing the three pairs of metals segregation as simultaneous equations. Binary segregation energies also matched closely with that are reported in the literature. An interactive tool was developed to aid the analysis of a large amount of data. Moreover, an analytical method of segregation was also solved to compare the obtained

results. It is concluded that the analytical model although predicted qualitatively similar results, it still requires further development and improvement.

This work allows one to understand the change in surface composition that will occur for a CuAgAu catalyst. Such an understanding permits one to tailor the surface composition by starting with a different bulk composition to reach the target surface composition. Future work can be aimed towards Monte Carlo simulations in a different ensemble or a more detailed AgAu segregation behavior. The change in composition can then be employed to the bigger problem of the reaction starting with Propylene adsorption on the surface.

References

- [1] Feng Cheng, Xiang He, Zhao-Xu Chen, and Yu-Gai Huang. Kinetic Monte Carlo simulation of surface segregation in Pd–Cu alloys. *Journal of Alloys and Compounds*, 648:1090–1096, 2015. doi: 10.1016/j.jallcom.2015.05.286. URL <https://doi.org/10.1016/j.jallcom.2015.05.286>.
- [2] B. C. Han, A. Van der Ven, G. Ceder, and Bing-Joe Hwang. Surface segregation and ordering of alloy surfaces in the presence of adsorbates. *Physical Review B*, 72(20):205409, 2005. doi: 10.1103/physrevb.72.205409. URL <https://doi.org/10.1103/physrevb.72.205409>.
- [3] John R. Kitchin, Karsten Reuter, and Matthias Scheffler. Alloy surface segregation in reactive environments: First-principles atomistic thermodynamics study of Ag₃Pd(111)in oxygen atmospheres. *Physical Review B*, 77(7):075437, 2008. doi: 10.1103/physrevb.77.075437. URL <https://doi.org/10.1103/physrevb.77.075437>.
- [4] Carl A. Menning and Jingguang G. Chen. General trend for adsorbate-induced segregation of subsurface metal atoms in bimetallic surfaces. *The Journal of Chemical Physics*, 130(17):174709, 2009. doi: 10.1063/1.3125926. URL <https://doi.org/10.1063/1.3125926>.
- [5] Donald McLean and A Maradudin. Grain boundaries in metals. *PhT*, 11(7):35, 1958.
- [6] M. A. Hoffmann and P. Wynblatt. Equilibrium surface composition of ternary alloys. *Metallurgical Transactions A*, 20(2):215–223, 1989. doi: 10.1007/bf02670247. URL <https://doi.org/10.1007/bf02670247>.
- [7] Roald Hoffmann. A chemical and theoretical way to look at bonding on surfaces. *Reviews of Modern Physics*, 60(3):601–628, 1988. doi: 10.1103/

- revmodphys.60.601. URL <https://doi.org/10.1103/revmodphys.60.601>.
- [8] M. A. Hoffmann and P. Wynblatt. Surface composition of ternary Cu–Ag–Au alloys: Part I. experimental results. *Metallurgical Transactions A*, 22(8):1833–1840, 1991. doi: 10.1007/bf02646507. URL <https://doi.org/10.1007/bf02646507>.
- [9] M. A. Hoffmann and P. Wynblatt. Surface composition of ternary Cu–Ag–Au alloys: Part II. A comparison of experiment with theoretical models. *Metallurgical Transactions A*, 22(8):1841–1848, 1991. doi: 10.1007/bf02646508. URL <https://doi.org/10.1007/bf02646508>.
- [10] Brian Good, Guillermo H. Bozzolo, and Phillip B. Abel. Surface segregation in ternary alloys. *Surface Science*, 454-456:602–607, 2000. doi: 10.1016/s0039-6028(00)00283-1. URL [https://doi.org/10.1016/s0039-6028\(00\)00283-1](https://doi.org/10.1016/s0039-6028(00)00283-1).
- [11] P. Wynblatt and R.C. Ku. Surface energy and solute strain energy effects in surface segregation. *Surface Science*, 65(2):511–531, 1977. doi: 10.1016/0039-6028(77)90462-9. URL [https://doi.org/10.1016/0039-6028\(77\)90462-9](https://doi.org/10.1016/0039-6028(77)90462-9).
- [12] R. Defay, I. Prigogine, A. Bellemans, and Everett D.H. *Surface Tension and Adsorption*. Wiley, 1966. URL <https://books.google.com/books?id=teF-zAEACAAJ>.
- [13] Meng Zhao, Willem G. Sloof, and Amarante J. Böttger. Modelling of surface segregation for palladium alloys in vacuum and gas environments. *International Journal of Hydrogen Energy*, 43(4):2212–2223, 2018. doi: 10.1016/j.ijhydene.2017.12.039. URL <https://doi.org/10.1016/j.ijhydene.2017.12.039>.

- [14] Meng Zhao, Johannes C. Brouwer, Willem G. Sloof, and Amarante J. Böttger. Surface segregation of ternary alloys: Effect of the interaction between solute elements. *Advanced Materials Interfaces*, 7(6):1901784, 2020. doi: 10.1002/admi.201901784. URL <https://doi.org/10.1002/admi.201901784>.
- [15] Richard M. Lambert, Federico J. Williams, Rachael L. Cropley, and Alejandra Palermo. Heterogeneous alkene epoxidation: Past, present and future. *Journal of Molecular Catalysis A: Chemical*, 228(1-2):27–33, 2005. doi: 10.1016/j.molcata.2004.09.077. URL <https://doi.org/10.1016/j.molcata.2004.09.077>.
- [16] Lei Cheng, Chunrong Yin, Faisal Mehmood, Bin Liu, Jeffrey Greeley, Sungsik Lee, Byeongdu Lee, Sönke Seifert., Randall E. Winans, Detre Teschner, Robert Schlögl, Stefan Vajda, and Larry A. Curtiss. Reaction mechanism for direct propylene epoxidation by alumina-supported silver aggregates: the role of the particle/support interface. *ACS Catalysis*, 4 (1):32–39, 2013. doi: 10.1021/cs4009368. URL <https://doi.org/10.1021/cs4009368>.
- [17] J Lu, J Bravosuarez, A Takahashi, M Haruta, and S Oyama. In situ uv-vis studies of the effect of particle size on the epoxidation of ethylene and propylene on supported silver catalysts with molecular oxygen. *Journal of Catalysis*, 232(1):85–95, 2005. doi: 10.1016/j.jcat.2005.02.013. URL <https://doi.org/10.1016/j.jcat.2005.02.013>.
- [18] Y. Lei, F. Mehmood, S. Lee, J. Greeley, B. Lee, S. Seifert, R. E. Winans, J. W. Elam, R. J. Meyer, P. C. Redfern, D. Teschner, R. Schlogl, M. J. Pellin, L. A. Curtiss, and S. Vajda. Increased silver activity for direct propylene epoxidation via subnanometer size effects. *Science*, 328(5975): 224–228, 2010. doi: 10.1126/science.1185200. URL <https://doi.org/10.1126/science.1185200>.

- [19] Xiang Zheng, Qing Zhang, Yanglong Guo, Wangcheng Zhan, Yun Guo, Yunsong Wang, and Guanzhong Lu. Epoxidation of propylene by molecular oxygen over supported Ag–Cu bimetallic catalysts with low Ag loading. *Journal of Molecular Catalysis A: Chemical*, 357:106–111, 2012. doi: 10.1016/j.molcata.2012.01.027. URL <https://doi.org/10.1016/j.molcata.2012.01.027>.
- [20] Xiang Zheng, Yang-Long Guo, Yun Guo, Qing Zhang, Xiao-Hui Liu, Li Wang, Wang-Cheng Zhan, and Guan-Zhong Lu. Epoxidation of propylene by molecular oxygen over unsupported AgCu_x bimetallic catalyst. *Rare Metals*, 34(7):477–490, 2015. doi: 10.1007/s12598-015-0500-y. URL <https://doi.org/10.1007/s12598-015-0500-y>.
- [21] Xiang Feng, Xuezhi Duan, Gang Qian, Xinggui Zhou, De Chen, and Weikang Yuan. Insights into size-dependent activity and active sites of Au nanoparticles supported on TS-1 for propene epoxidation with H_2 and O_2 . *Journal of Catalysis*, 317:99–104, 2014. doi: 10.1016/j.jcat.2014.05.006. URL <https://doi.org/10.1016/j.jcat.2014.05.006>.
- [22] Xiang Feng, Zhaoning Song, Yibin Liu, Xiaobo Chen, Xin Jin, Wenjuan Yan, Chaohe Yang, Jun Luo, Xinggui Zhou, and De Chen. Manipulating gold spatial location on titanium silicalite-1 to enhance the catalytic performance for direct propene epoxidation with H_2 and O_2 . *ACS Catalysis*, 8(11):10649–10657, 2018. doi: 10.1021/acscatal.8b02836. URL <https://doi.org/10.1021/acscatal.8b02836>.
- [23] Xiang Feng, Jia Yang, Xuezhi Duan, Yueqiang Cao, Bingxu Chen, Wenyao Chen, Dong Lin, Gang Qian, De Chen, Chaohe Yang, and Xinggui Zhou. Enhanced catalytic performance for propene epoxidation with H_2 and O_2 over bimetallic Au–Ag/uncalcined titanium silicate-1 catalysts. *ACS Catalysis*, 8(9):7799–7808, 2018. doi: 10.1021/acscatal.8b01324. URL <https://doi.org/10.1021/acscatal.8b01324>.

- [24] Brian Good and Guillermo Bozzolo. Surface composition of alloys via BFS atomistic Monte Carlo simulation. *Surface Science*, 507-510:730–735, 2002. doi: 10.1016/s0039-6028(02)01344-4. URL [https://doi.org/10.1016/s0039-6028\(02\)01344-4](https://doi.org/10.1016/s0039-6028(02)01344-4).
- [25] Thomas B. Blank, Steven D. Brown, August W. Calhoun, and Douglas J. Doren. Neural network models of potential energy surfaces. *The Journal of Chemical Physics*, 103(10):4129–4137, 1995. doi: 10.1063/1.469597. URL <https://doi.org/10.1063/1.469597>.
- [26] Jörg Behler and Michele Parrinello. Generalized Neural-Network representation of high-dimensional potential-energy surfaces. *Physical Review Letters*, 98(14):146401, 2007. doi: 10.1103/physrevlett.98.146401. URL <https://doi.org/10.1103/physrevlett.98.146401>.
- [27] Tianyu Gao and John R. Kitchin. Modeling palladium surfaces with density functional theory, neural networks and molecular dynamics. *Catalysis Today*, 312:132–140, 2018. doi: 10.1016/j.cattod.2018.03.045. URL <https://doi.org/10.1016/j.cattod.2018.03.045>.
- [28] Jacob R. Boes, Mitchell C. Groenenboom, John A. Keith, and John R. Kitchin. Neural network and reaxff comparison for Au properties. *International Journal of Quantum Chemistry*, 116(13):979–987, 2016. doi: 10.1002/qua.25115. URL <https://doi.org/10.1002/qua.25115>.
- [29] Jacob R. Boes and John R. Kitchin. Modeling segregation on AuPd(111) surfaces with density functional theory and Monte Carlo simulations. *The Journal of Physical Chemistry C*, 121(6):3479–3487, 2017. doi: 10.1021/acs.jpcc.6b12752. URL <https://doi.org/10.1021/acs.jpcc.6b12752>.
- [30] Nongnuch Artrith and Jörg Behler. High-dimensional neural network potentials for metal surfaces: a prototype study for copper. *Physical*

Review B, 85(4):045439, 2012. doi: 10.1103/physrevb.85.045439. URL <https://doi.org/10.1103/physrevb.85.045439>.

- [31] Martín Leandro Paleico and Jörg Behler. Global optimization of copper clusters at the ZnO(1010) surface using a DFT-based neural network and genetic algorithms. *The Journal of Chemical Physics*, 153(5):054704, 2020. doi: 10.1063/5.0014876. URL <https://doi.org/10.1063/5.0014876>.
- [32] Nongnuch Artrith, Björn Hiller, and Jörg Behler. Neural network potentials for metals and oxides - first applications to copper clusters at zinc oxide. *physica status solidi (b)*, 250(6):1191–1203, 2012. doi: 10.1002/pssb.201248370. URL <https://doi.org/10.1002/pssb.201248370>.
- [33] Samad Hajinazar, Junping Shao, and Aleksey N. Kolmogorov. Stratified construction of neural network based interatomic models for multi-component materials. *Physical Review B*, 95(1):014114, 2017. doi: 10.1103/physrevb.95.014114. URL <https://doi.org/10.1103/physrevb.95.014114>.
- [34] Samad Hajinazar, Ernesto D Sandoval, Aiden J Cullo, and Aleksey N Kolmogorov. Multitribe evolutionary search for stable cupdag nanoparticles using neural network models. *Physical Chemistry Chemical Physics*, 21(17):8729–8742, 2019.
- [35] Jörg Behler. First principles neural network potentials for reactive simulations of large molecular and condensed systems. *Angewandte Chemie International Edition*, 56(42):12828–12840, 2017. doi: 10.1002/anie.201703114. URL <https://doi.org/10.1002/anie.201703114>.
- [36] G. Kresse and J. Hafner. Ab Initio molecular dynamics for liquid metals. *Physical Review B*, 47(1):558–561, 1993. doi: 10.1103/physrevb.47.558. URL <https://doi.org/10.1103/physrevb.47.558>.

- [37] G. Kresse and J. Hafner. Ab initio molecular-dynamics simulation of the liquid-metal-amorphous-semiconductor transition in germanium. *Physical Review B*, 49(20):14251–14269, 1994. doi: 10.1103/physrevb.49.14251. URL <https://doi.org/10.1103/physrevb.49.14251>.
- [38] G. Kresse and J. Furthmüller. Efficient iterative schemes for ab-initio total-energy calculations using a plane-wave basis set. *Physical Review B*, 54(16):11169–11186, 1996. doi: 10.1103/physrevb.54.11169. URL <https://doi.org/10.1103/physrevb.54.11169>.
- [39] John P. Perdew, Kieron Burke, and Matthias Ernzerhof. Generalized gradient approximation made simple. *Physical Review Letters*, 77(18):3865–3868, 1996. doi: 10.1103/physrevlett.77.3865. URL <https://doi.org/10.1103/physrevlett.77.3865>.
- [40] John P. Perdew, Kieron Burke, and Matthias Ernzerhof. Generalized gradient approximation made simple [phys. rev. lett. 77, 3865 (1996)]. *Physical Review Letters*, 78(7):1396–1396, 1997. doi: 10.1103/physrevlett.78.1396. URL <https://doi.org/10.1103/physrevlett.78.1396>.
- [41] P. E. Blöchl. Projector augmented-wave method. *Physical Review B*, 50(24):17953–17979, 1994. doi: 10.1103/physrevb.50.17953. URL <https://doi.org/10.1103/physrevb.50.17953>.
- [42] G. Kresse and D. Joubert. From ultrasoft pseudopotentials to the projector augmented-wave method. *Physical Review B*, 59(3):1758–1775, 1999. doi: 10.1103/physrevb.59.1758. URL <https://doi.org/10.1103/physrevb.59.1758>.
- [43] Hendrik J. Monkhorst and James D. Pack. Special points for brillouin-zone integrations. *Physical Review B*, 13(12):5188–5192, 1976. doi: 10.1103/physrevb.13.5188. URL <https://doi.org/10.1103/physrevb.13.5188>.

- [44] Stefan Grimme. Semiempirical GGA-type density functional constructed with a long-range dispersion correction. *Journal of computational chemistry*, 27(15):1787–1799, 2006.
- [45] Stefan Grimme, Jens Antony, Stephan Ehrlich, and Helge Krieg. A consistent and accurate ab initio parametrization of density functional dispersion correction (DFT–D) for the 94 elements H–Pu. *The Journal of Chemical Physics*, 132(15):154104, 2010. doi: 10.1063/1.3382344. URL <https://doi.org/10.1063/1.3382344>.
- [46] Jess Wellendorff, Keld T. Lundgaard, Andreas Møgelhøj, Vivien Petzold, David D. Landis, Jens K. Nørskov, Thomas Bligaard, and Karsten W. Jacobsen. Density functionals for surface science: Exchange-correlation model development with bayesian error estimation. *Physical Review B*, 85(23):235149, 2012. doi: 10.1103/physrevb.85.235149. URL <https://doi.org/10.1103/physrevb.85.235149>.
- [47] Jörg Behler. Atom-centered symmetry functions for constructing high-dimensional neural network potentials. *The Journal of Chemical Physics*, 134(7):074106, 2011. doi: 10.1063/1.3553717. URL <https://doi.org/10.1063/1.3553717>.
- [48] Matthias Rupp, Alexandre Tkatchenko, Klaus-Robert Müller, and O. Anatole von Lilienfeld. Fast and accurate modeling of molecular atomization energies with machine learning. *Physical Review Letters*, 108(5):058301, 2012. doi: 10.1103/physrevlett.108.058301. URL <https://doi.org/10.1103/physrevlett.108.058301>.
- [49] Felix Faber, Alexander Lindmaa, O. Anatole von Lilienfeld, and Rickard Armiento. Crystal structure representations for machine learning models of formation energies. *International Journal of Quantum Chemistry*, 115

- (16):1094–1101, 2015. doi: 10.1002/qua.24917. URL <https://doi.org/10.1002/qua.24917>.
- [50] Haoyan Huo and Matthias Rupp. Unified representation of molecules and crystals for machine learning, 2017.
- [51] Albert P. Bartók, Risi Kondor, and Gábor Csányi. On representing chemical environments. *Physical Review B*, 87(18):184115, 2013. doi: 10.1103/physrevb.87.184115. URL <https://doi.org/10.1103/physrevb.87.184115>.
- [52] Lauri Himanen, Marc O.J. Jäger, Eiaki V. Morooka, Filippo Federici Canova, Yashasvi S. Ranawat, David Z. Gao, Patrick Rinke, and Adam S. Foster. Dscribe: Library of descriptors for machine learning in materials science. *Computer Physics Communications*, 247:106949, 2020. doi: 10.1016/j.cpc.2019.106949. URL <https://doi.org/10.1016/j.cpc.2019.106949>.
- [53] Adam Paszke, Sam Gross, Francisco Massa, Adam Lerer, James Bradbury, Gregory Chanan, Trevor Killeen, Zeming Lin, Natalia Gimelshein, Luca Antiga, Alban Desmaison, Andreas Kopf, Edward Yang, Zachary DeVito, Martin Raison, Alykhan Tejani, Sasank Chilamkurthy, Benoit Steiner, Lu Fang, Junjie Bai, and Soumith Chintala. Pytorch: An imperative style, high-performance deep learning library. In H. Wallach, H. Larochelle, A. Beygelzimer, F. d'Alché-Buc, E. Fox, and R. Garnett, editors, *Advances in Neural Information Processing Systems 32*, pages 8024–8035. Curran Associates, Inc., 2019. URL <http://papers.neurips.cc/paper/9015-pytorch-an-imperative-style-high-performance-deep-learning-library.pdf>.
- [54] Ask Hjorth Larsen, Jens Jørgen Mortensen, Jakob Blomqvist, Ivano E

Castelli, Rune Christensen, Marcin Dułak, Jesper Friis, Michael N Groves, Bjørk Hammer, Cory Hargus, Eric D Hermes, Paul C Jennings, Peter Bjerre Jensen, James Kermode, John R Kitchin, Esben Leonhard Kolsbjerg, Joseph Kubal, Kristen Kaasbjerg, Steen Lysgaard, Jón Bergmann Maronsson, Tristan Maxson, Thomas Olsen, Lars Pastewka, Andrew Peterson, Carsten Rostgaard, Jakob Schiøtz, Ole Schütt, Mikkel Strange, Kristian S Thygesen, Tejs Vegge, Lasse Vilhelmsen, Michael Walter, Zhenhua Zeng, and Karsten W Jacobsen. The atomic simulation environment—a python library for working with atoms. *Journal of Physics: Condensed Matter*, 29(27):273002, 2017. URL <http://stacks.iop.org/0953-8984/29/i=27/a=273002>.

- [55] S. R. Bahn and K. W. Jacobsen. An object-oriented scripting interface to a legacy electronic structure code. *Comput. Sci. Eng.*, 4(3):56–66, MAY-JUN 2002. ISSN 1521-9615. doi: 10.1109/5992.998641.
- [56] A. V. Ruban, H. L. Skriver, and J. K. Nørskov. Surface segregation energies in transition-metal alloys. *Physical Review B*, 59(24):15990–16000, 1999. doi: 10.1103/physrevb.59.15990. URL <https://doi.org/10.1103/physrevb.59.15990>.
- [57] Carson Sievert. *Interactive Web-Based Data Visualization with R, plotly, and shiny*. Chapman and Hall/CRC, 2020. ISBN 9781138331457. URL <https://plotly-r.com>.
- [58] G. Tréglia, B. Legrand, F. Ducastelle, A. Saúl, C. Gallis, I. Meunier, C. Mottet, and A. Senhaji. Alloy surfaces: Segregation, reconstruction and phase transitions. *Computational Materials Science*, 15(2):196–235, 1999. doi: 10.1016/s0927-0256(99)00004-x. URL [https://doi.org/10.1016/s0927-0256\(99\)00004-x](https://doi.org/10.1016/s0927-0256(99)00004-x).
- [59] J. Y. Wang, J. du Plessis, J. J. Terblans, and G. N. van Wyk. Equi-

librium surface segregation of silver to the low-index surfaces of a copper single crystal. *Surface and Interface Analysis*, 28(1):73–76, 1999. doi: 10.1002/(sici)1096-9918(199908)28:1<73::aid-sia621>3.0.co; 2-e. URL [https://doi.org/10.1002/\(sici\)1096-9918\(199908\)28:1<73::aid-sia621>3.0.co;2-e](https://doi.org/10.1002/(sici)1096-9918(199908)28:1<73::aid-sia621>3.0.co;2-e).

- [60] J.Y Wang, J du Plessis, J.J Terblans, and G.N van Wyk. The discontinuous surface transition in the Cu(111)(Ag) binary segregating system. *Surface Science*, 419(2-3):197–206, 1999. doi: 10.1016/s0039-6028(98)00790-0. URL [https://doi.org/10.1016/s0039-6028\(98\)00790-0](https://doi.org/10.1016/s0039-6028(98)00790-0).
- [61] V.I. Razumovskiy, S.V. Divinski, and L. Romaner. Solute segregation in Cu: DFT vs. experiment. *Acta Materialia*, 147:122–132, 2018. doi: 10.1016/j.actamat.2018.01.011. URL <https://doi.org/10.1016/j.actamat.2018.01.011>.
- [62] Daniela S. Mainardi and Perla B. Balbuena. Surface segregation in bimetallic nanoclusters: Geometric and thermodynamic effects. *International Journal of Quantum Chemistry*, 85(4-5):580–591, 2001. doi: 10.1002/qua.1524. URL <https://doi.org/10.1002/qua.1524>.
- [63] Edgar Völker, Federico J. Williams, Ernesto J. Calvo, Timo Jacob, and David J. Schiffrin. O₂ induced Cu surface segregation in Au–Cu alloys studied by angle resolved XPS and DFT modelling. *Physical Chemistry Chemical Physics*, 14(20):7448, 2012. doi: 10.1039/c2cp40565b. URL <https://doi.org/10.1039/c2cp40565b>.
- [64] Chunrong Yin, Zhitao Guo, and Andrew J. Gellman. Surface segregation across ternary alloy composition space: Cu_xAu_yPd_{1-x-y}. *The Journal of Physical Chemistry C*, page acs.jpcc.0c02058, 2020. doi: 10.1021/acs.jpcc.0c02058. URL <https://doi.org/10.1021/acs.jpcc.0c02058>.

- [65] M A Vasiliev. Surface effects of ordering in binary alloys. *Journal of Physics D: Applied Physics*, 30(22):3037–3070, 1997. doi: 10.1088/0022-3727/30/22/002. URL <https://doi.org/10.1088/0022-3727/30/22/002>.
- [66] L. Vitos, A.V. Ruban, H.L. Skriver, and J. Kollár. The surface energy of metals. *Surface Science*, 411(1):186 – 202, 1998. ISSN 0039-6028. doi: [https://doi.org/10.1016/S0039-6028\(98\)00363-X](https://doi.org/10.1016/S0039-6028(98)00363-X). URL <http://www.sciencedirect.com/science/article/pii/S003960289800363X>.
- [67] S. Fain and J. McDavid. Work-function variation with alloy composition: Ag–Au. *Physical Review B*, 9(12):5099–5107, 1974. doi: 10.1103/physrevb.9.5099. URL <https://doi.org/10.1103/physrevb.9.5099>.
- [68] R Bouwman, L.H Toneman, M.A.M Boersma, and R.A Van Santen. Surface enrichment in AgAu alloys. *Surface Science*, 59(1):72–82, 1976. doi: 10.1016/0039-6028(76)90292-2. URL [https://doi.org/10.1016/0039-6028\(76\)90292-2](https://doi.org/10.1016/0039-6028(76)90292-2).
- [69] S.H Overbury and G.A Somorjai. The surface composition of the silver-gold system by auger electron spectroscopy. *Surface Science*, 55(1):209–226, 1976. doi: 10.1016/0039-6028(76)90385-x. URL [https://doi.org/10.1016/0039-6028\(76\)90385-x](https://doi.org/10.1016/0039-6028(76)90385-x).
- [70] T.S. King and R.G. Donnelly. Surface compositions and composition profiles of AgAu (100), (110), and (111) surfaces determined quantitatively by auger electron spectroscopy. *Surface Science*, 151(2-3):374–399, 1985. doi: 10.1016/0039-6028(85)90382-6. URL [https://doi.org/10.1016/0039-6028\(85\)90382-6](https://doi.org/10.1016/0039-6028(85)90382-6).
- [71] G.C Nelson. Determination of the surface versus bulk composition of silver-gold alloys by low energy ion scattering spectroscopy. *Surface Sci-*

- ence, 59(1):310–314, 1976. doi: 10.1016/0039-6028(76)90310-1. URL [https://doi.org/10.1016/0039-6028\(76\)90310-1](https://doi.org/10.1016/0039-6028(76)90310-1).
- [72] M. J. Kelley, D. G. Swartzfager, and V. S. Sundaram. Surface segregation in the Ag–Au and Pt–Cu systems. *Journal of Vacuum Science and Technology*, 16(2):664–667, 1979. doi: 10.1116/1.570052. URL <https://doi.org/10.1116/1.570052>.
- [73] G.N. Derry and R. Wan. Comparison of surface structure and segregation in AgAu and NiPd alloys. *Surface Science*, 566-568(nil):862–868, 2004. doi: 10.1016/j.susc.2004.06.022. URL <https://doi.org/10.1016/j.susc.2004.06.022>.
- [74] Guillermo Bozzolo, Jorge E. Garcés, and Gregory N. Derry. Atomistic modeling of segregation and bulk ordering in Ag-Au alloys. *Surface Science*, 601(9):2038–2046, 2007. doi: 10.1016/j.susc.2007.02.035. URL <https://doi.org/10.1016/j.susc.2007.02.035>.
- [75] Lei Deng, Wangyu Hu, Huiqiu Deng, Shifang Xiao, and Jianfeng Tang. Au–Ag bimetallic nanoparticles: Surface segregation and atomic-scale structure. *The Journal of Physical Chemistry C*, 115(23):11355–11363, 2011. doi: 10.1021/jp200642d. URL <https://doi.org/10.1021/jp200642d>.
- [76] Fuyi Chen and Roy L. Johnston. Charge transfer driven surface segregation of gold atoms in 13-atom Au–Ag nanoalloys and its relevance to their structural, optical and electronic properties. *Acta Materialia*, 56(10):2374–2380, 2008. doi: 10.1016/j.actamat.2008.01.048. URL <https://doi.org/10.1016/j.actamat.2008.01.048>.
- [77] Lauro Oliver Paz-Borbón, Roy L. Johnston, Giovanni Barcaro, and Alessandro Fortunelli. Structural motifs, mixing, and segregation effects in 38-atom binary clusters. *The Journal of Chemical Physics*, 128

- (13):134517, 2008. doi: 10.1063/1.2897435. URL <https://doi.org/10.1063/1.2897435>.
- [78] A. L. Gould, C. J. Heard, A. J. Logsdail, and C. R. A. Catlow. Segregation effects on the properties of (AuAg)147. *Phys. Chem. Chem. Phys.*, 16(39):21049–21061, 2014. doi: 10.1039/c4cp00753k. URL <https://doi.org/10.1039/c4cp00753k>.
- [79] Vlasta Bonačić-Koutecký, Jaroslav Burda, Roland Mitrić, Maofa Ge, Giuseppe Zampella, and Piercarlo Fantucci. Density functional study of structural and electronic properties of bimetallic silver-gold clusters: Comparison with pure gold and silver clusters. *The Journal of Chemical Physics*, 117(7):3120–3131, 2002. doi: 10.1063/1.1492800. URL <https://doi.org/10.1063/1.1492800>.
- [80] J. J. Rehr, E. Zaremba, and W. Kohn. Van der waals forces in the noble metals. *Physical Review B*, 12(6):2062–2066, 1975. doi: 10.1103/physrevb.12.2062. URL <https://doi.org/10.1103/physrevb.12.2062>.
- [81] Jiří Klimeš and Angelos Michaelides. Perspective: Advances and challenges in treating van der waals dispersion forces in density functional theory. *The Journal of Chemical Physics*, 137(12):120901, 2012. doi: 10.1063/1.4754130. URL <https://doi.org/10.1063/1.4754130>.
- [82] Werner Reckien, Florian Janetzko, Michael F. Peintinger, and Thomas Bredow. Implementation of empirical dispersion corrections to density functional theory for periodic systems. *Journal of Computational Chemistry*, 33(25):2023–2031, 2012. doi: 10.1002/jcc.23037. URL <https://doi.org/10.1002/jcc.23037>.
- [83] Tomas Bučko, Jurgen Hafner, Sébastien Lebegue, and János G Angyán. Improved description of the structure of molecular and layered crystals:

- ab initio DFT calculations with van der waals corrections. *The Journal of Physical Chemistry A*, 114(43):11814–11824, 2010.
- [84] Sandra Hoppe and Stefan Müller. A first principles study on the electronic origins of silver segregation at the Ag–Au (111) surface. *Journal of Applied Physics*, 122(23):235303, 2017. doi: 10.1063/1.5017959. URL <https://doi.org/10.1063/1.5017959>.
- [85] Deepika Priyadarshini, Petro Kondratyuk, Yoosuf N. Picard, Bryan D. Morreale, Andrew J. Gellman, and James B. Miller. High-throughput characterization of surface segregation in Cu_xPd_{1-x} alloys. *The Journal of Physical Chemistry C*, 115(20):10155–10163, 2011. doi: 10.1021/jp201793d. URL <https://doi.org/10.1021/jp201793d>.